

First-Principles calculation of atomic hydrogen adsorption on Be(10 $\bar{1}$ 0) thin films

Ping Zhang, Hong-Zhou Song

Institute of Applied Physics and Computational Mathematics, P.O. Box 8009, Beijing 100088, P.R. China

We present a first-principles study of the atomic hydrogen adsorption onto the Be(10 $\bar{1}$ 0) thin film. There are two types of Be(10 $\bar{1}$ 0) surfaces according to the interlayer spacing between the surface and its nearest-neighbor layer. We show that the H adsorption features on these two kinds of surfaces are remarkably different. The work function, averaged electrostatic potential, and the local charge density consistently show that the charge is transferred from H to Be for L-type (see the text below) surfaces, while the transfer process is inverted for S-type surfaces.

PACS numbers: 73.61.-r, 73.20.At, 73.21.Ac,

Beryllium belongs to the *sp*-bonded “simple metal”, however, it is far from nearly-free-electron like and has many anomalous properties. For example, compared to its close neighbor, Mg, the *c/a* ratio for hcp Be has a very nonideal value of 1.57 (1.62 for Mg), showing the directional bonding in Be. The bonding energy of Be is surprisingly strong with cohesive energy 3.32 eV/atom. Also, the Debye temperature is very high, with a value of 1440 K (Mg: 400 K), and thus quantum effects should be more pronounced for Be in determining its zero-temperature structural properties¹. The electronic structure of Be is very profound by the following unique properties: the bulk Be shows a very low density of states (DOS) at the Fermi energy (E_F) and thus exhibits some degree of covalent-like bonding^{2,3}. However, the Be(0001) and Be(10 $\bar{1}$ 0) surfaces have been shown, both experimentally and theoretically, to be a nearly-free-electron system⁴. This large metallic enhancement in the DOS originates from the surface states⁵, which accounts for roughly 80% of the local DOS at E_F in the outermost layer. This peculiarly large surface-to-bulk ratio of the local DOS (LDOS) at E_F has been shown to provide the basic framework to understand many observed surface properties which deviate substantially from the bulk, including abnormally large surface core level shifts^{6,7,8,9,10,11,12}, giant surface Friedel oscillations^{13,14,15,16}, large surface expansion^{17,18}, and enhancement of electron-phonon interaction^{19,20,21,22,23,24}.

In the present study we present a detailed first-principles study of the adsorption properties of atomic hydrogen onto Be(10 $\bar{1}$ 0) thin films. The interaction of H with Be(0001) surface has been theoretically studied by Feibelman and Stumpf²⁵ who showed that H prefers ordinary hcp threefold sites at low coverages, while at high coverage with long-range ordering inevitably taken into account, the H adsorption has been shown to lead Be(0001) surface to $(\sqrt{3} \times \sqrt{3})R30^\circ$ reconstruction²⁶. To the best of our knowledge, the adsorption of H on Be(10 $\bar{1}$ 0) surface has not been studied before. Considering that the clean Be(10 $\bar{1}$ 0) surface, and many novel effects including surface core level shifts, electron-phonon interaction, and large surface expansion have been extensively revealed, we feel it necessary to give a de-

tailed study of adsorption properties of H adsorption onto Be(10 $\bar{1}$ 0) surface. Also, it is an interesting task to investigate the effect of H adsorption on the various kinds of enhancement phenomena in Be surfaces and we will leave it for future study.

The calculations were carried out using the Vienna *ab initio* simulation package²⁷ based on density-functional theory with ultrasoft pseudopotentials²⁸ and plane waves. In the present film calculations, free-standing Be(10 $\bar{1}$ 0) films in periodic slab geometries were employed. The periodic slabs are separated by a vacuum region equal to 20 Å. In all the calculations below, a surface (1×1) was employed for the supercell slab. The Brillouin-zone integration was performed using Monkhorse-Pack scheme²⁹ with a $11 \times 11 \times 1$ *k*-point grid, and the plane-wave energy cutoff was set 300 eV. Furthermore, the generalized gradient approximation (GGA) with PW-91 exchange-correlation potential has been employed with all atomic configurations fully relaxed. A Fermi broadening of 0.05 eV was chosen to smear the occupation of the bands around E_F by a finite-temperature Fermi function and extrapolating to $T = 0$ K. Optimized atomic geometries are achieved when the forces on all the unconstrained atoms are in magnitude smaller than 0.01 eV/Å. First the total energy of the bulk hcp Be was calculated to obtain the bulk lattice constants. The calculated *a*- and *c*-lattice parameters are 2.272 Å and 3.544 Å, comparable well with experimental³⁰ values of 2.285 Å and 3.585 Å, respectively.

Choosing the (10 $\bar{1}$ 0) plane as the basal plane, then the unit cell of the bulk Be, including four atoms inside, has an orthorhombic structure with the basis vectors given by $\mathbf{a}_1 = (c, 0, 0)$, $\mathbf{a}_2 = (0, a, 0)$, $\mathbf{a}_3 = (0, 0, \sqrt{3}a)$. In terms of this basis set, the positions of four atoms in bulk hcp Be are given by $(0, 0, 0)$, $(0.5, 0.5, 1/6)$, $(0, 0.5, 0.5)$, and $(0.5, 0, 2/3)$. One can see that the (10 $\bar{1}$ 0) surface of hcp Be can be terminated either with a short first interlayer spacing, $d_s = \sqrt{3}a/6$, or with a long one, $d_l = \sqrt{3}a/3$. The preferred termination has been found experimentally and theoretically to be the short one with d_s ³¹. During the following discussions, we will call a Be(10 $\bar{1}$ 0) monolayer as a S layer if the interlayer spacing between this layer and its nearest-neighbor layer (from below) is d_s . In the same way, a Be(10 $\bar{1}$ 0) monolayer will be termed in

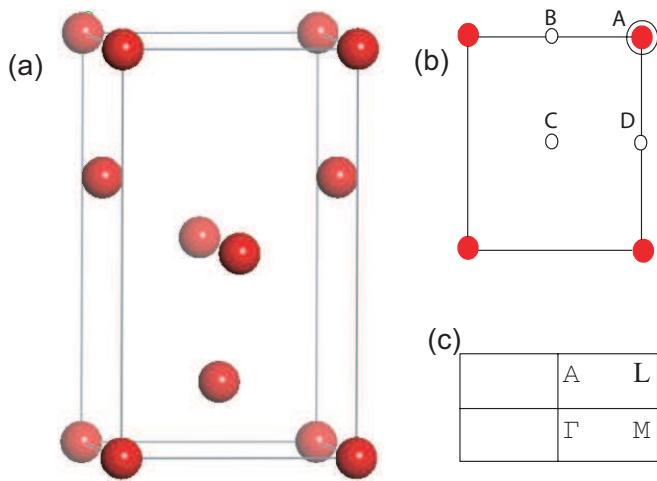


FIG. 1: (Color online) (a) Bulk unit cell of hcp Be along $[10\bar{1}0]$ direction; (b) The four probable adsorption sites (A, B, C, and D) for atomic hydrogen on Be($10\bar{1}0$). The red circles denote the topmost surface Be atoms; (c) the Be($10\bar{1}0$) surface Brillouin zone.

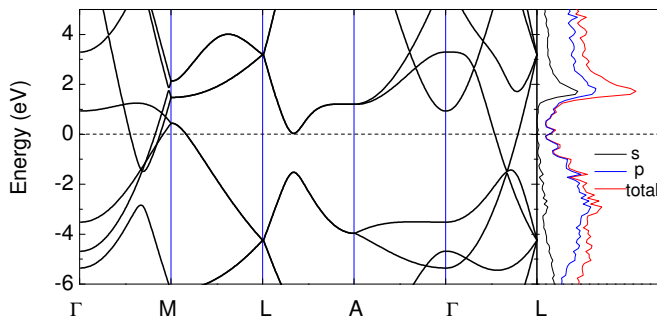


FIG. 2: (Color online) GGA energy bands and density of electron states (right panel) of hcp bulk Be. The dashed line denotes Fermi level.

this paper as a L layer if the interlayer spacing between this layer and its nearest-neighbor layer (from below) is d_l .

The band structure and the DOS of bulk Be with unit cell in Fig. 1(a) are shown in Fig. 2. One can see that the density of electronic states for bulk Be resembles somewhat that of a semiconductor since it has a minimum at the Fermi energy. This makes Be different from its close neighbors, such as Mg, whose band property is nearly free-electron like. The bulk Be bands display a direct gap in a large range of the Brillouin zone, unlike Mg. Mg has a filled state at Γ with energy $\simeq 1.3$ eV, while the corresponding Be state is above the Fermi energy and its band is nearly flat. This band is the source of both the low density of states near the Fermi energy and the high peak above the Fermi energy¹. Although the electronic configuration of elemental Be is $1s^2 2s^2$, one can see from Fig. 2 that the p -orbital component in bulk Be plays a

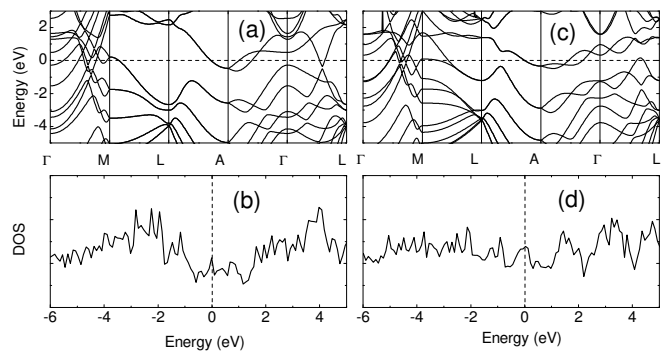


FIG. 3: Energy bands and density of electron states of Be($10\bar{1}0$) thin films with 10 monolayers included in the slabs. The left panels denote the case that the bottom and top surfaces of the slab are L-type, while the right panels denote the case of S-type surfaces.

main role around E_F . The bonding properties of hcp Be is anisotropic, which can be seen by the fact that the c/a ratio (1.56) is one of the most contracted for hcp metals (for Mg, $c/a \simeq 1.62$). Thus out-of-plane neighbors have shorter bonds than in-plane neighbors. Another evidence of this anisotropy is that the contribution of p_x and p_y orbitals to the DOS is different from that of p_z component³².

The above-mentioned “semiconducting” metallic picture for bulk Be is prominently changed in the case of Be($10\bar{1}0$) surfaces. To illustrate this change, the electronic structure properties of Be($10\bar{1}0$) thin films with two kinds of surfaces are shown in Fig. 3, wherein the left panels give the band structure and density of electron states for a structure with L-type surfaces, while the right panels show the results for a structure with L-type surfaces. The number of Be($10\bar{1}0$) monolayers in these two slabs has been fixed to be 10. Compared to the bulk results shown in Fig. 2, it reveals in Fig. 3 that (i) the sharp DOS peak above Fermi level in Fig. 2 becomes broad for Be($10\bar{1}0$) thin films, resulting in a prominent enhancement of the DOS at E_F with respect to the bulk case. This phenomenon of high density of surface states at E_F was previously reported for Be(0001)⁴, and was also noticed in other metal films such as W(110) and Mo(110)³³; (ii) Compared to the L-type surfaces, the enhancement of DOS at E_F is more prominent for S-type surfaces, implying that the metallic behavior in S-type Be($10\bar{1}0$) surfaces is more strong than in L-type surfaces. Also, the band structure for S-type surfaces deviates more far from the bulk band structure than that for L-type surfaces. Thus the preference of S-type surfaces to L-type surfaces, as observed in experiment³¹, is the result of this more metallic behavior of S-type surfaces; (iii) The band structure around Γ point is characterized by a series of subbands which can be well fit by $E_n + \hbar^2(k_x^2 + k_y^2)/2m^*$ with the effective mass m^* , demonstrating from another aspect the quasi-2D free-electron

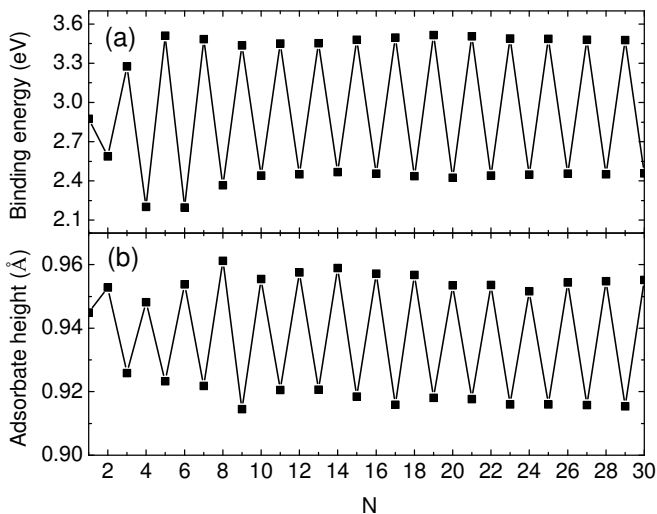


FIG. 4: Calculated (a) binding energy of H adatom and (b) adsorbate height as a function of the number of Be(10 $\bar{1}0$) monolayers in the slab.

character in the Be(10 $\bar{1}0$) thin film, which is contrary to the bulk Be.

Now we focus our attention to the atomic hydrogen adsorption onto Be(10 $\bar{1}0$). Before we study the adsorption properties as a function of the thickness of Be(10 $\bar{1}0$) thin films, we need to determine the energetically favourable adsorption site. Since the preference of adsorption site is not sensitive to the thickness of the substrate, thus to look for this preference, it is sufficient to give a study on the slabs with fixed thickness of the Be(10 $\bar{1}0$) film. As mentioned above, there are two kinds of Be(10 $\bar{1}0$) surfaces, namely the S- and L-type surfaces. For both of these two kinds of surfaces the thickness of the Be(10 $\bar{1}0$) film is fixed to be 9 monolayers. We choose four most probable adsorption sites, which have been indicated in Fig. 1(b). The binding energy is calculated using the following equation: Binding energy [atomic H] = $-(E[\text{H}/\text{Be}(10\bar{1}0)] - E[\text{Be}(10\bar{1}0)] - 2E[\text{H}])/2$ where $E[\text{H}/\text{Be}(10\bar{1}0)]$ is the total energy of a slab which consists of 9 layers of Be atoms and one H atom on each side, $E[\text{Be}(10\bar{1}0)]$ is total energy of the slab without H atoms, and $E[\text{H}]$ is total energy of a free H atom which is put in a 10 $\text{\AA} \times 10 \text{\AA} \times 10 \text{\AA}$ supercell. As a result, the calculated binding energy of atomic H for these four different adsorption configurations in Fig. 1(b) is 2.38 eV (A), 3.51 eV (B), 3.42 eV (C), 2.44 eV (D) for the L-type surface, and 1.44 eV (A), 2.2 eV (B), 1.61 eV (C), 2.06 eV (D) for the S-type surface, showing a clear preference for B site adsorption for both kinds of surfaces. At this site the H atoms interact strongly with the dangling bond like p orbitals of the Be surface atoms. Those orbitals point out of the surface.

After finding the preferred atomic H adsorption site, we give a series of calculations for the binding energy of the H adsorbate as a function of the thickness of Be(10 $\bar{1}0$)

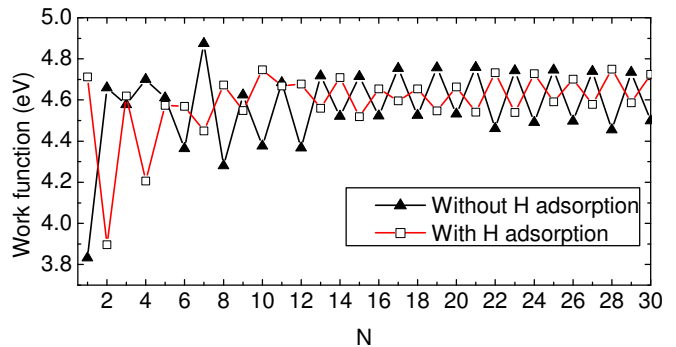


FIG. 5: (Color online) Work function of Be(10 $\bar{1}0$) thin film with (open squares) and without (filled triangles) H adsorption as a function of the number of Be monolayers in the slab. The bottom layer has been fixed to be L-type

thin films. The results are summarized in Fig. 4(a). One can see that the binding energy oscillates when increasing the Be monolayers in the slab. The peaks in the oscillations correspond to the case that the topmost Be(10 $\bar{1}0$) monolayer is L-type, while the valley values are for the H adsorption onto the S-type surfaces. In experiment this dependence can be observed by investigating the dependence of H coverage on the monolayers of Be(10 $\bar{1}0$) thin films. The cohesion between the H overlayer and the L-type Be(10 $\bar{1}0$) surface is so strong that the majority of available electrons at the interface participate in the metallic behavior with only a minority participating in covalent H-Be bonds. For H adsorption onto the S-type Be(10 $\bar{1}0$) surface, whereas, the binding energy is not so strong, implying that the surface bonding is dominated by the covalent hybridization between H s and Be p orbitals with less ionic behavior. The height of H adatom above the Be(10 $\bar{1}0$) surface is plotted in Fig. 4(b), also showing an oscillatory variance between the S- and L-type surfaces. The typical H adsorbate height is 0.915 \AA for L-type surfaces and 0.955 \AA for S-type surfaces. The lower value of adsorbate height for L-type surfaces compared to S-type surfaces implies more attraction between adatom H and topmost Be atoms for L-type surfaces.

Figure 5 shows the work function of the Be(10 $\bar{1}0$) film as a function of the number of Be monolayers in the slab with and without H adsorption, respectively. During the calculation the bottom Be layer in the slabs is fixed to be L-type. In the absence of H adsorption, one can see that the work function for the clean Be(10 $\bar{1}0$) surfaces is oscillatory with respect to the thickness of the film. There is a critical value for the number N of Be(10 $\bar{1}0$) monolayers in the slab, separating Fig. 5 into two regimes: when $N < 6$, we find that the work function is much larger for the S-type surfaces than for the L-type surfaces, resulting in the clear interlayer oscillations of the work function as shown in Fig. 4. For convenience of expression, we call this kind of oscillation as SL-type; When the value of N is larger than 6, the work function for the Be(10 $\bar{1}0$)

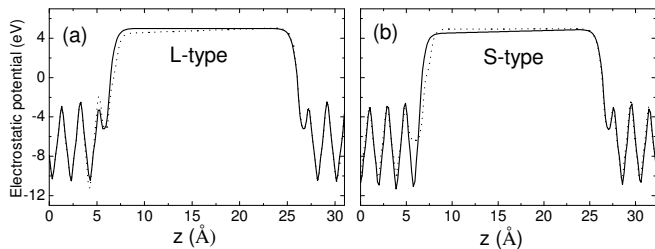


FIG. 6: Planar-averaged electrostatic potential of clean (solid line) and H-adsorbed (dotted line) Be(10 $\bar{1}0$) thin films. The left and right panels are the results for S- and L-type Be(10 $\bar{1}0$) surfaces, respectively.

L-type surfaces turns out to be much larger than that for the S-type surfaces, resulting in a converted inter-layer oscillations of the work function as shown in Fig. 5. Similarly we call this kind of oscillation as LS-type. In the presence of H adsorption, one can see from Fig. 5 that the situation is totally inverted: in the case of ultra-thin films ($N < 6$), the work function is oscillatory in a way that its value is larger for L-type surfaces than for S-type surfaces, while in the case of $N > 6$, the work function for L-type surfaces is much lower than that for the S-type surfaces.

Clearly, in the absence (presence) of H adsorption, the transition from a SL (LS) oscillation at $N < 6$ to a LS (SL) oscillation at $N > 6$ is due to the atomic relaxation process of Be(10 $\bar{1}0$) monolayers in the slab. In fact, in another series of calculation, by fixing the bottom Be surface in the slabs to be S-type, we have found that the critical value for the oscillation transition is decreased to be $N = 3$. This reduction of critical value of N is not difficult to understand when one recalls that the preferred Be(10 $\bar{1}0$) surface is S-type³¹. Thus we arrive at the conclusion that the steady oscillation mode of Be(10 $\bar{1}0$) work function in the absence (presence) of H adsorption is LS- (SL-) type.

The change of oscillation mode of work function by the presence of H adsorption indicates a partially ionic character of the H-Be bond, i.e., charge is transferred between H and Be. However, the transfer direction is remarkably different for the two types of surfaces. It is generally believed that the work functions increase (decrease) when the negatively (positively) charged adatom adsorbs above the surface. For H adatom on L-type Be(10 $\bar{1}0$) surfaces, since the work function is reduced, thus charge is transferred from H to Be, leading to a polarization of electronic charge away from the H adlayer towards the Be surface. For H adsorption on S-type Be(10 $\bar{1}0$) surfaces, whereas, since the work function is increased, thus in this case charge is transferred from Be to H and the H adsorbate is negatively charged.

To show more clearly this conversion from LS- to SL-type oscillations in work function by the presence of H adsorption, we further plot in Fig. 6 the xy -averaged

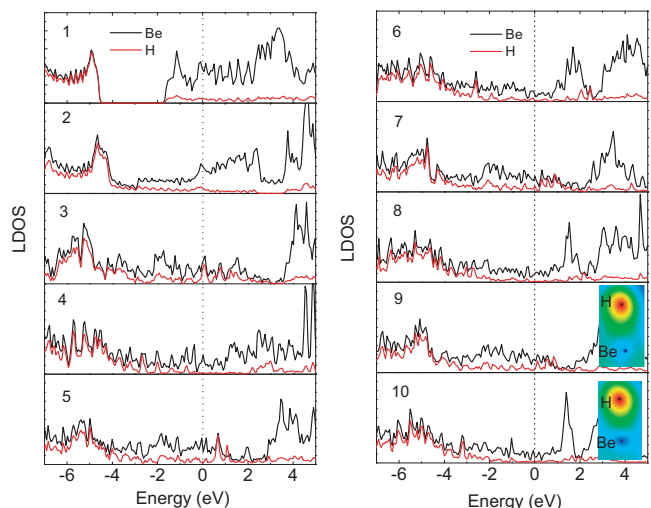


FIG. 7: (Color online) Calculated local density of states of H adatom and topmost Be atom. The number of Be(10 $\bar{1}0$) monolayers in the slabs is shown in the figure. The even numbers (2, 4, 6, 8, 10) denote the cases that the topmost Be(10 $\bar{1}0$) monolayer is L-type, while the odd numbers denote the cases of S-type surfaces

electrostatic potentials $\bar{V}(z)$ as a function of z coordinate normal to the Be(10 $\bar{1}0$) surface for typical L-type [Fig. 6(a)] and S-type [Fig. 6(b)] Be(10 $\bar{1}0$) surfaces. The solid lines Fig. 6 are the results for the clean surfaces while the dotted lines account for the H adsorption. From Fig. 6(a) one can see that in the presence of H adsorption, the electrostatic potential for L-type surface curves down towards the surface, showing the existence of a surface dipole due to the charge transfer from H to Be. For the S-type surface, as shown in Fig. 6(b), however, one can see that $\bar{V}(z)$ curves up towards the surface by the H adsorption. In this case, the surface dipole, due to the charge transfer from Be to H, points to the opposite and increases the work function, which subsequently displays an SL-type oscillation mode.

Now we turn to a full study of the surface electronic structure of H-covered Be(10 $\bar{1}0$). For this we calculate the local density of states (LDOS) through projections of the total wave function onto atoms of interest within the Wigner-Seitz spheres around them. Figure 7 plots a series of LDOS of H adatom layer and the topmost Be(10 $\bar{1}0$) layer for different thickness of Be thin films. The even numbers (2, 4, 6, 8, 10) in Fig. 7 denote the cases that the topmost Be(10 $\bar{1}0$) monolayer is L-type, while the odd numbers denote the cases of S-type surfaces. One can see that the LDOS is largely different for the two types of Be(10 $\bar{1}0$) surfaces. The magnitude of LDOS at Fermi level is higher for S-type surfaces than that for L-type surfaces, which means that the charge transfer between H and Be is more active for S-type surfaces than for L-type surfaces. This also can be seen in the insets in Fig. 7, which plot the local charge den-

sities for S- and L-type surfaces, respectively. One can see that compared to the case of H adsorption on L-type surfaces, more electrons populate around H adatom on S-type surfaces. Thus we arrive at the conclusion that the H adatom on S-type surfaces behaves more negatively charged. This is consistent with the result in Fig. 6 which shows that the charge transfers from H to Be for L-type surfaces, while the transfer process is inverted for S-type surfaces.

In summary, the H adsorption on Be(10 $\bar{1}$ 0) thin films has been studied by density-functional theory pseudopotential plane-wave calculations. The dependence of electronic structure, binding energy, and workfunction upon the thickness of the film has been fully investigated. We have shown that (i) the S-type Be(10 $\bar{1}$ 0) surface is more metallic than the L-type surface; (ii) The H-adsorption induced charge transfer process is different for the two kinds Be(10 $\bar{1}$ 0) surfaces. While the charge is transferred from H to Be for L-type surface, it is transferred from

Be to H for S-type surface; (iii) In the absence of H adsorption, the work function displays a LS-type oscillation mode as a function of the thickness of the Be(10 $\bar{1}$ 0) film. In the presence of H adsorption, the oscillation mode is transformed to be SL-type, i.e., the value of work function is high for S-type surface and low for L-type surface. This transformation of the oscillation mode of the work function is closely related to the charge transfer process mentioned in (ii). We expect this prominent change in the work function and charge transfer will have a significant effect on the other relevant physical properties³⁴ in Be(10 $\bar{1}$ 0) surface with H adsorption.

Acknowledgments

This work was partially supported by CNSF No. 10544004 and 10604010.

-
- ¹ M. Lazzeri, Ph.D. Thesis, Oct. 1999 SISSA, Trieste.
- ² D.A. Papaconstantopoulos, *Handbook of Band Structure of Elemental Solids* (Plenum, New York, 1986).
- ³ I. Yu. Sklyadneva, E.V. Chulkov, W.-D. Schöne, V.M. Silkin, R. Keyling, and P.M. Echenique, *Phys. Rev. B* **71**, 174302 (2005).
- ⁴ E.V. Chulkov, V.M. Silkin, and E.N. Shirykalov, *Surf. Sci.* **188**, 287 (1987); Ph. Hofmann, R. Stumpf, V.M. Silkin, E.V. Chulkov, and E.W. Plummer, *ibid.* **355**, L278 (1996).
- ⁵ T. Balasubramanian *et al.*, *Phys. Rev. B* **64**, 205401 (2001).
- ⁶ P.J. Feibelman and R. Stumpf, *Phys. Rev. B* **50**, 17480 (1994); P.J. Feibelman, *ibid.* **48**, 11270 (1993).
- ⁷ M. Aldén, H.L. Skriver, and B. Johansson, *Phys. Rev. B* **50**, 12118 (1994).
- ⁸ L.I. Johansson, P.-A. Glans, and T. Balasubramanian, *Phys. Rev. B* **58**, 3621 (1998).
- ⁹ S. Lizzit *et al.*, *Phys. Rev. Lett.* **81**, 3271 (1998).
- ¹⁰ J.-H. Cho, K.S. Kim, S.-H. Lee, M.-H. Kang, and Z. Zhang, *Phys. Rev. B* **61**, 9975 (2000).
- ¹¹ J. Rundgren, *Phys. Rev. B* **68**, 125405 (2003).
- ¹² P.-A. Glans, L.I. Johansson, T. Balasubramanian, and R. J. Blake, *Phys. Rev. B* **70**, 033408 (2004).
- ¹³ L.I. Johansson, H. I. P. Johansson, J. N. Andersen, E. Lundgren, and R. Nyholm, *Phys. Rev. Lett.* **71**, 2453 (1993).
- ¹⁴ P.T. Sprunger, L. Petersen, E.W. Plummer, E. Løegsgaard, and F. Besenbacher, *Science* **275**, 1764 (1997).
- ¹⁵ Ph. Hofmann, B.G. Briner, M. Doering, H.-P. Rust, E.W. Plummer, and A. M. Bradshaw, *Phys. Rev. Lett.* **79**, 265 (1997).
- ¹⁶ B.G. Briner, Ph. Hofmann, M. Doering, H.-P. Rust, E.W. Plummer, and A.M. Bradshaw, *Phys. Rev. B* **58**, 13931 (1998).
- ¹⁷ M. Lazzeri and S. de Gironcoli, *Phys. Rev. Lett.* **81**, 2096 (1998); *Phys. Rev. B* **65**, 245402 (2005).
- ¹⁸ I. Vobornik, J. Fujii, M. Mulazzi, G. Panaccione, M. Hochstrasser, and G. Rossi, *Phys. Rev. B* **72**, 165424 (2005).
- ¹⁹ M. Hengsberger, D. Purdie, P. Segovia, M. Garnier, and Y. Baer, *Phys. Rev. Lett.* **83**, 592 (1999).
- ²⁰ T. Balasubramanian, P.-A. Glans, and L. I. Johansson, *Phys. Rev. B* **61**, 12709 (2000).
- ²¹ S.-J. Tang, Ismail, P.T. Sprunger, and E.W. Plummer, *Phys. Rev. B* **65**, 235428 (2002).
- ²² Ismail, Ph. Hofmann, A.P. Baddorf, and E.W. Plummer, *Phys. Rev. B* **66**, 245414 (2002).
- ²³ A. Eiguren, S. de Gironcoli, E.V. Chulkov, P.M. Echenique, and E. Tosatti, *Phys. Rev. Lett.* **91**, 166803 (2003).
- ²⁴ J. Shi *et al.*, *Phys. Rev. Lett.* **92**, 186401 (2004).
- ²⁵ R. Stumpf and P.J. Feibelman, *Phys. Rev. B* **51**, 13748 (1995).
- ²⁶ K. Pohl and E.W. Plummer, *Phys. Rev. B* **59**, R5324 (1999).
- ²⁷ G. Kresse and J. Furthmüller, *Phys. Rev. B* **54**, 11169 (1996).
- ²⁸ D. Vanderbilt, *Phys. Rev. B* **41**, 7892 (1990).
- ²⁹ H.J. Monkhorst and J.D. Pack, *Phys. Rev. B* **13**, 5188 (1976).
- ³⁰ V.M. Amonenko, V. Ye. Ivanov, G.F. Tikhinskij, and V.A. Finkel, *Phys. Met. Metallogr.* **14**, 47 (1962).
- ³¹ Ph. Hofmann *et al.*, *Surf. Sci.* **355**, L278 (1996); *Phys. Rev. B* **53**, 13715 (1996).
- ³² M.Y. Chou, Pui K. Lam, and M.L. Cohen, *Phys. Rev. B* **28**, 4179 (1983).
- ³³ E. Rotenberg, J. Schaefer, and S.D. Kevan, *Phys. Rev. Lett.* **84**, 2925 (2000).
- ³⁴ E.W. Plummer, J. Shi, S.-J. Tang, E. Rotenberg, and S.D. Kevan, *Prog. in Surf. Sci.* **74**, 251 (2003).